Angewandte Chemie
Eine Zeitschrift der Gesellschaft Deutscher Chemiker

Supporting Information

69451 Weinheim, Germany

Population Shuffling of Protein Conformations**

Colin A. Smith, David Ban, Supriya Pratihar, Karin Giller, Claudia Schwiegk, Bert L. de Groot, Stefan Becker, Christian Griesinger, and Donghan Lee**

anie_201408890_sm_miscellaneous_information.pdf

Supplementary Methods

Sample Preparation

Perdeuterated, ^{15}N-labeled ubiquitin and GB3 with the selective $^{13}CHD_2$ labeling in δ1-Ile, δ1,δ2-Leu, and γ1,γ2-Val were expressed in *E. coli* adapted to 100 % D_2O minimal medium supplemented with D_7-glucose as carbon source and ^{15}N-NH_4Cl as nitrogen source with the addition of the precursors 2-keto-3-D_2-4-^{13}C,D_2-butyrate and 2-keto-3-methyl-D_3-3-D_1-4-^{13}C,D_2-butyrate (Cambridge Isotope Laboratories) 1 hour before the induction of protein expression[14]. For the production of perdeuterated, ^{15}N-labeled GB3, the precursors were omitted. The purification of recombinant ubiquitin and GB3 was performed as described before[28,29]. All the protein samples were used at a concentration of 3 mM in 50 mM sodium phosphate buffer of pH 6.5, containing 100 mM NaCl and 0.05% sodium azide.

Nuclear Magnetic Resonance

All ubiquitin experiments were collected at 277 K and all GB3 experiments were collected at 275 K. Data consisting of relaxation rates ($R_{1\rho}$), effective field strengths (ω_{eff}), and tilt angles (θ) were fit with the following equation

$$R_{1\rho}/\sin^2(\theta) = R_2 + \Phi_{ex}\,\tau_{ex} / (1 + \tau_{ex}^2\,\omega_{eff}^2) \qquad \text{(S1)}$$

with the derived parameters being the intrinsic transverse relaxation time (R_2), conformational amplitude (Φ_{ex}), and lifetime of the exchange process (τ_{ex}) (Figure S2-5). Standard errors in the fitted parameters were determined in two different ways. The first method used the formal definition of the standard error derived from the fit residuals. The second method used a Monte Carlo bootstrapping procedure with 1000 independent fits using $R_{1\rho}$ values with Gaussian noise added according to the $R_{1\rho}/\sin^2(\theta)$ standard errors. For each reported parameter, the method giving the greater error was used. The following criteria were used to select nuclei showing significant chemical exchange: 1) The standard errors of all fit parameters must be no greater than 50% of the magnitude of the parameter. 2) The difference

in mean value of the first four $R_{1\rho}/\sin^2(\theta)$ data points and the mean value of the last four data points must be greater than four times the mean value of the $R_{1\rho}/\sin^2(\theta)$ standard error. 3) The F-test confidence level must be greater than 99% for a fit to equation S1 vs. one without dispersion (i.e. $R_{1\rho}/\sin^2(\theta) = R_2$).

Methyl ^{13}C experiments were performed on a uniformly deuterated, selectively methyl labeled $^{13}CHD_2$ sample in D_2O, in which only δ1-Ile, δ1,δ2-Leu, and γ1,γ2-Val were labeled. ^{13}C field strengths were calibrated by measuring perturbed $^1J_{CH}$ with a [^1H,^{13}C]-HSQC in which ^{13}C-CW decoupling was applied off-resonance during acquisition (Figure S1). The CHD_2 labeling scheme provides a simple AX spin system to probe methyl ^{13}C nuclei. This facilitated the use of an off-resonance $R_{1\rho}$ experiment analogous to ones developed for backbone ^{15}N nuclei[30,31]. The current scheme incorporated ^2H decoupling during t_1 evolution, and cross-relaxation between CSA/DD interactions was controlled by placing ^1H 180° pulses at T/4 and 3T/4 during the relaxation delay where T is the length of the relaxation delay[30]. Measurements were conducted by varying the offset and amplitude of the spin-lock. Spin-lock strengths (ν_{rf}) were varied from 1000 to 16,000 Hz (ubiquitin) or 17,000 Hz (GB3), and offsets (Ω) by ±10 ppm from the carrier frequency which was set at ~15 ppm. The use of high power ν_{rf} was conducted in a similar fashion as previously[13] where the length of the temperature compensation block was varied based on the given spin-lock amplitude and duration of the relaxation period so that the same amount of power was deposited for every transient regardless of the employed field strength and duration. Temperature compensation was achieved by applying the maximum spin-lock amplitude off-resonance on the ^{13}C channel during the recycle delay. Movement of magnetization to the correct offset position before application of the spin-lock was controlled by a 4 ms adiabatic pulse[31]. The maximum duration a given spin-lock was applied for was 125 ms. In total, 128 ($t_{1,max}$ = 42.4 ms, ubiquitin) or 64 ($t_{1,max}$ = 53.1ms, GB3) and 1024 ($t_{2,max}$ = 139.2 ms) complex

points in the indirect and direct dimensions, respectively, were acquired. A recycle delay of 3.0 (ubiquitin) or 4.0 seconds (GB3) was used yielding a total measurement time of ~51 minutes per point. All methyl ^{13}C $R_{1\rho}$ experiments were conducted on a Bruker spectrometer operating at a ^{1}H frequency of 600 MHz with a QCI cryo-probehead.

Initially, ^{13}C dispersion curves were fitted with a description of $R_{1\rho}$ that considers fast exchange ($R_1 \cos^2(\theta) + R_2 \sin^2(\theta) + \Phi (\tau_{ex}/(1 + (\tau_{ex}^2 \omega_{eff}^2)) \sin^2(\theta)$) and one that considers the absence of exchange ($R_1 \cos^2(\theta) + R_2 \sin^2(\theta)$), where R_1 and R_2 are the intrinsic longitudinal and transverse relaxation rates, Φ is the conformational amplitude, τ_{ex} is the lifetime of the exchange process, and ω_{eff} is the effective field ($\omega_{eff} = ((2 \pi \nu_{rf})^2 + (2 \pi \Omega)^2)^{1/2}$). In order to minimize the effect of R_1, only points that were measured with a $\sin(\theta)$ greater than 0.96 were accepted. This maintained a R_1 contribution of less than 8% to the observed $R_{1\rho}$ rate and resulted in approximately 18 (ubiquitin) or 13 points (GB3) per dispersion curve. Dispersion curves fitted with this criteria yielded R_1 values of ~0 s^{-1}. This allowed us to reformulate the observed dispersion by removing the contribution from R_1 as $R_{1\rho}/\sin^2(\theta)$.

$^{1}H^{N}$ (all resonances having significant RD are shown in Figure 1) and methyl ^{1}H dispersion experiments were recorded with the perdeuterated ^{15}N-labeled GB3 sample and the same samples as the ^{13}C methyl experiments, respectively. For the measurement of ^{1}H $R_{1\rho}$ the experiments follow previous methods[13]. Spin-lock frequencies were varied from 1000 to 10,000 Hz (ubiquitin), 25,000 Hz (GB3 $^{1}H^{N}$), and 27,000 Hz (GB3 methyl ^{1}H) and were calibrated by measuring ^{1}H 90° pulse lengths at their corresponding power levels. Field strengths and offsets were chosen in a way that the tilt-angles of 35° were used for all points in order to minimize the NOE and ROE effects that can lead to pseudo dispersion profiles[13]. The experiments were carried out in an interleaved fashion where the employed delay, field strength, and offset were randomly varied. With the current experimental parameters the

overall change in the temperature was less than 1 K. Relaxation rates were determined using a three point (ubiquitin) and a four point (GB3) sampling scheme with spin-lock relaxation delays of 5, 65, and 125 ms (ubiquitin) and 2, 45, 95, 125 ms (GB3), respectively. Rate errors were estimated using residuals from the three point fits. Mean $R_{1\rho}$ and ω_{eff} values were determined using equations 5 and 6 from reference [13]. All $^1H^N$ and methyl ^1H $R_{1\rho}$ experiments were conducted on a Bruker spectrometer operating at a ^1H frequency of 600 MHz.

Expected Φ_{ex} for 3-state rotamer jumps of valine

For valine three different rotameric states can exist in solution, the trans (t), gauche$^+$ (p), and gauche$^-$ (m)[32]. We were interested in determining if the observed experimental conformational amplitudes for valine residues that show relaxation dispersion are consistent with discrete three-state rotameric jumps. This scheme will also be applicable for any discrete three-state rotamer jump. The kinetic scheme can be modeled as,

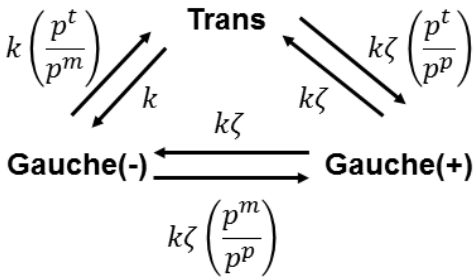

where k is the overall transition rate, and ζ is the term used to scale whether a step from one to the other is kinetically faster or slower than the other steps. The kinetic transition matrix (K) is

$$KP = \begin{pmatrix} -k(1+\zeta) & k\left(\frac{p^t}{p^m}\right) & k\zeta\left(\frac{p^t}{p^p}\right) \\ k & -k\left(\frac{p^t}{p^m}+\zeta\right) & k\zeta\left(\frac{p^m}{p^p}\right) \\ k\zeta & k\zeta & -k\zeta\left(\frac{p^t+p^m}{p^p}\right) \end{pmatrix} \begin{pmatrix} p^t \\ p^m \\ p^p \end{pmatrix} \quad \text{(S2)}$$

and whose eigenvalues ($\lambda_{1\text{-}3}$) are 0, $-k\zeta/p^p$, and $-k(p^t/p^m + (1+\zeta))$, respectively. The

conditional probabilities can be evaluated as

$$P(m,t \mid l,0) = \sum_{n}^{3} \Lambda_{mn} \Lambda_{nl}^{-1} e^{\lambda_n t} \tag{S3}$$

in which Λ is a matrix of eigenvectors and Λ^{-1} its inverse of the kinetic matrix, K. The a priori conditional probabilities are known from the initial conditions where $P_a = \lim_{t\to\infty} P(a,t \mid b,0) \quad a,b \in [1,3]$. The correlation function is then given by[33]

$$C(t) = \langle \delta(0)\delta(t) \rangle = \sum_{l,m=1}^{3} P_l \left(\sum_{n}^{3} \Lambda_{mn} \Lambda_{nl}^{-1} e^{\lambda_n t} \right) \delta_l \delta_m \tag{S4}$$

Evaluation of equation S4 yields

$$C(t) = \left(p^m \delta_m + p^p \delta_p + p^t \delta_t \right)^2 + \frac{p^m p^t \Delta\delta_{m-t}{}^2}{p^m + p^t} e^{\lambda_2 t} + \frac{p^p (p^m \Delta\delta_{m-p} + p^t \Delta\delta_{t-p})}{p^m + p^t} e^{\lambda_3 t} \tag{S5}$$

The first term corresponds to the square of the average chemical shift (δ) and is time invariant and does not cause relaxation[33]. After Fourier transform we retain only the second and third terms from equation S5 which gives

$$R_{ex} = \frac{p^m p^t \Delta\delta_{m-t}{}^2}{p^m + p^t} \cdot \frac{\tau_2}{1 + (\gamma B_1 \tau_2)^2} + \frac{p^p (p^m \Delta\delta_{m-p} + p^t \Delta\delta_{t-p})}{p^m + p^t} \cdot \frac{\tau_3}{1 + (\gamma B_1 \tau_3)^2} \tag{S6}$$

In equation S6, τ_2 and τ_3 correspond to $1/\lambda_2$ and $1/\lambda_3$, γB_1 is the employed field strength for a given $R_{1\rho}$ experiment, $p^{t,m,p}$ correspond to the populations in the trans, gauche$^-$, and gauche$^+$ conformations, and the term preceding the Lorentzians are the Φ values. $\Delta\delta_x$ are the difference in chemical shifts between rotameric states (x=m-t, m-p, t-p). From the kinetic matrix, ζ can be set to match any desired exchange lifetime, and therefore does not affect the calculation of the expected conformational amplitudes. However, the least negative eigenvalue, whose lifetime is given by τ_3, will only contribute to observed dispersion and its prefactor will be the expected Φ_{ex}. We can now evaluate the expected ubiquitin and GB3 Φ_{ex} values for three-state discrete rotamer jumps using RDC derived populations[12,34] and chemical shifts derived from a DFT based hypersurface[32]. In Table S2, all calculated values

still exceed the measured Φ_{ex} for the RD data from all valines indicating that discrete rotameric jumps cannot account for the observed dispersion.

Quantification of Population Shuffling

Since discrete rotamer jumps cannot reconcile the observed conformational amplitudes for methyl ^{13}C nuclei (see Main text), we instead propose a new model that doesn't assume rotamer jumps occurring on the timescale of the observed exchange lifetime (τ_{ex}), but significantly faster ($<<\tau_{ex}$).

For a two state fast exchange process with an exchange rate of τ_{ex}, Φ_{ex} can be described in terms of the populations of the two states (p_A and p_B) which we now call macrostates:

$$\Phi_{ex} = p_A p_B \Delta\omega^2 \tag{S7}$$

with the chemical shift difference ($\Delta\omega$) defined

$$\Delta\omega = \omega_B - \omega_A \tag{S8}$$

where ω_A and ω_B are the average chemical shifts of each macrostate. Each average chemical shift (ω_i) is composed of the population average of unique chemical shifts (δ_j)

$$\omega_i = \omega_0 \sum_{j=1}^{N} p_i^j \, \delta_j \tag{S9}$$

where p_i^j represents the conditional probability of having chemical shift δ_j given that the system is in macrostate $i = A \; or \; B$ and $\sum_{j=1}^{N} p_i^j = 1$. If it assumed that the γ-effect dominates the chemical shifts, only two chemical shift values are possible and equation S9 can be rewritten as

$$\Delta\omega/\omega_0 = (p_B^1\delta_1 + p_B^2\delta_2) - (p_A^1\delta_1 + p_A^2\delta_2) = (p_B^1 - p_A^1)\delta_1 + (p_B^2 - p_A^2)\delta_2 \tag{S10}$$

Because $(p_B^2 - p_A^2) = -(p_B^1 - p_A^1)$, this can be rearranged

$$\Delta\omega/\omega_0 = (p_B^1 - p_A^1)(\delta_1 - \delta_2) = \Delta p_{A\to B}^1 \Delta\delta_\gamma \tag{S11}$$

where $\Delta p^1_{A\to B}$ is the change in conditional probability of chemical shift δ_1 and $\Delta\delta_\gamma$ is the difference between the chemical shift values.

If equation S11 is substituted into equation S7 and solved for $\Delta p^1_{A\to B}$, then the changes in populations between macrostates can be quantified from Φ_{ex} values using the equation

$$|\Delta p^1_{A\to B}| = \frac{1}{\omega_0 \Delta\delta_\gamma}\sqrt{\frac{\Phi_{ex}}{p_A p_B}} \tag{S12}$$

The minimum $\Delta p^1_{A\to B}$ is produced when $p_A = p_B = 0.5$. As the populations become more unequal, the resulting $\Delta p^1_{A\to B}$ becomes larger and larger.

Depending on the side chain and the specific nucleus, different rotameric states may have unique chemical shifts. For leucine ^{13}Cδ1 the chemical shift of the trans (t) state is unique but the gauche$^+$ (p) and gauche$^-$ (m) states are indistinguishable. Therefore we assign $p^1_i = p^t_i$ and $p^2_i = p^p_i + p^m_i$, and use the ^{13}Cδ1 Φ_{ex} value to quantify $\Delta p^t_{A\to B}$. For leucine ^{13}Cδ2, only the gauche$^+$ rotameric state has a unique chemical shift so we assign $p^1_i = p^p_i$ and determine $\Delta p^p_{A\to B}$. The valine ^{13}Cγ1 and ^{13}Cγ2 chemical shifts depend primarily on the populations of the gauche$^+$ and gauche$^-$ states, respectively[32]. Therefore we use the ^{13}Cγ1 Φ_{ex} to quantify $\Delta p^p_{A\to B}$ and ^{13}Cγ2 Φ_{ex} to quantify $\Delta p^m_{A\to B}$. Finally, for isoleucine the ^{13}Cδ1 chemical shift depends on the gauche$^-$ population[35], so we use that to quantify $\Delta p^m_{A\to B}$. For all methyl groups, a $\Delta\delta_\gamma$ of 5.5 ppm was used[35], which satisfied constraints over all modeled residues (Figure S7-S8).

Φ_{ex} can also be described using the N-site jump model[36] for cases described in the paragraph above:

$$\Phi_{ex} = \frac{1}{2N^2}\sum_{i,j=1}^{N}\left(\delta_j - \delta_i\right)^2 \tag{S13}$$

in which each interconversion event between states *i* or *j* is associated with a unique chemical shift value (δ_i). The δ_i can be expanded to include the fast rotamer jumps where

$$\delta_i = p^1_i\delta_1 + p^2_i\delta_2 \tag{S14}$$

Substituting equation S14 back into equation S13 yields

$$\Phi_{ex} = \frac{1}{2N^2}\sum_{i,j=1}^{N}\left(p_j^1\delta_1 + p_j^2\delta_2 - (p_i^1\delta_1 + p_i^2\delta_2)\right)^2 \tag{S15}$$

The term in the summation can be simplified to

$$\Phi_{ex} = \frac{1}{2N^2}\sum_{i,j=1}^{N}\left(\left(p_j^1 - p_i^1\right)\delta_1 + \left(p_j^2 - p_i^2\right)\delta_2\right)^2 \tag{S16}$$

and because $p_i^1 - p_j^1 = p_j^2 - p_i^2$ equation S16 is recast as

$$\Phi_{ex} = \frac{1}{2N^2}\sum_{i,j=1}^{N}\left(\Delta p_{i\to j}^1\delta_1 - \Delta p_{i\to j}^1\delta_2\right)^2 \tag{S17}$$

This yields the formulation for Φ_{ex} as

$$\Phi_{ex} = \frac{\left(\Delta\delta_\gamma\right)^2}{2N^2}\sum_{i,j=1}^{N}\left(\Delta p_{i\to j}^1\right)^2 \tag{S18}$$

Modeling Population Constraints

Carbon chemical shifts of leucine methyls 1 and 2 are, respectively,

$$\delta_1 = p_A p_A^t\delta_t + p_A p_A^p\delta_g + p_A p_A^m\delta_g + p_B p_B^t\delta_t + p_B p_B^p\delta_g + p_B p_B^m\delta_g \tag{S19}$$

$$\delta_2 = p_A p_A^t\delta_g + p_A p_A^p\delta_t + p_A p_A^m\delta_g + p_B p_B^t\delta_g + p_B p_B^p\delta_t + p_B p_B^m\delta_g \tag{S20}$$

p_A and p_B are populations of macrostates. p_A^t, p_A^p, and p_A^m are the respective conditional populations of trans, gauche$^+$, and gauche$^-$ within the *A* macrostate. p_B^t, p_B^p, and p_B^m are the respective conditional populations of trans, gauche$^+$, and gauche$^-$ within the *B* macrostate. δ_t and δ_g are chemical shifts for the position of trans and gauche, respectively. Thus, the difference between these two chemical shifts is

$$\Delta\delta = \delta_1 - \delta_2 = p_A p_A^t\Delta\delta_\gamma - p_A p_A^p\Delta\delta_\gamma + p_B p_B^t\Delta\delta_\gamma - p_B p_B^p\Delta\delta_\gamma \tag{S21}$$

where $\Delta\delta_\gamma = \delta_t - \delta_g$ is the g-gauche effect. This can be simplified as

$$\Delta\delta = [(p_A p_A^t + p_B p_B^t) - (p_A p_A^p + p_B p_B^p)\,]\Delta\delta_\gamma \tag{S22}$$

The amplitudes of relaxation dispersion for two methyl carbons when we have two macrostates are $\phi_{\delta 1} = p_A p_B(\Delta \mathrm{p}_{A\to B}^t)^2\left(\omega_\gamma\right)^2$ and $\phi_{\delta 2} = p_A p_B\left(\Delta \mathrm{p}_{A\to B}^p\right)^2\left(\omega_\gamma\right)^2$ where

$$\Delta \mathrm{p}_{A\to B}^{t} = p_A^t - p_B^t = \pm\sqrt{\frac{\phi_{\delta 1}}{p_A p_B (\omega_\gamma)^2}} \tag{S23}$$

$$\Delta \mathrm{p}_{A\to B}^{p} = p_A^p - p_B^p = \pm\sqrt{\frac{\phi_{\delta 2}}{p_A p_B (\omega_\gamma)^2}} \tag{S24}$$

and $\omega_\gamma = \gamma B_0 \Delta\delta_\gamma$. Other conditions are as follows:

$$p_A + p_B = 1$$

$$p_A^t + p_A^p + p_A^m = 1$$

$$p_B^t + p_B^p + p_B^m = 1$$

By solving these three equations with respect to p_A^t together with other conditions, the conditional populations can be obtained as:

$$p_A^t = p_A^t \tag{S25}$$

$$p_A^p = p_A^t - \frac{\Delta\delta}{\Delta\delta_\gamma} - p_B\left(\sqrt{\frac{\phi_{\delta 1}}{p_A p_B (\omega_\gamma)^2}} - \sqrt{\frac{\phi_{\delta 2}}{p_A p_B (\omega_\gamma)^2}}\right)$$

$$= p_A^t - \frac{\Delta\delta}{\Delta\delta_\gamma} - p_B\left(\Delta \mathrm{p}_{A\to B}^{t} - \Delta \mathrm{p}_{A\to B}^{p}\right) \tag{S26}$$

$$p_A^m = 1 - 2p_A^t + \frac{\Delta\delta}{\Delta\delta_\gamma} + p_B\left(\sqrt{\frac{\phi_{\delta 1}}{p_A p_B (\omega_\gamma)^2}} - \sqrt{\frac{\phi_{\delta 2}}{p_A p_B (\omega_\gamma)^2}}\right)$$

$$= 1 - 2p_A^t + \frac{\Delta\delta}{\Delta\delta_\gamma} + p_B\left(\Delta \mathrm{p}_{A\to B}^{t} - \Delta \mathrm{p}_{A\to B}^{p}\right) \tag{S27}$$

$$p_B^t = p_A^t - \sqrt{\frac{\phi_{\delta 1}}{p_A p_B (\omega_\gamma)^2}}$$

$$= p_A^t - \Delta \mathrm{p}_{A\to B}^{t} \tag{S28}$$

$$p_B^p = p_A^t - \frac{\Delta\delta}{\Delta\delta_\gamma} - \sqrt{\frac{\phi_{\delta 1}}{p_A p_B (\omega_\gamma)^2}} + p_A\left(\sqrt{\frac{\phi_{\delta 1}}{p_A p_B (\omega_\gamma)^2}} - \sqrt{\frac{\phi_{\delta 2}}{p_A p_B (\omega_\gamma)^2}}\right)$$

$$= p_A^t - \frac{\Delta\delta}{\Delta\delta_\gamma} - \Delta \mathrm{p}_{A\to B}^{t} + p_A\left(\Delta \mathrm{p}_{A\to B}^{t} - \Delta \mathrm{p}_{A\to B}^{p}\right)$$

$$= p_A^t - \frac{\Delta\delta}{\Delta\delta_\gamma} - p_B \Delta \mathrm{p}_{A\to B}^{t} - p_A \Delta \mathrm{p}_{A\to B}^{p} \tag{S29}$$

$$p_B^m = 1 - 2p_A^t + \frac{\Delta\delta}{\Delta\delta_\gamma} + 2\sqrt{\frac{\phi_{\delta 1}}{p_A p_B(\omega_\gamma)^2}} - p_A\left(\sqrt{\frac{\phi_{\delta 1}}{p_A p_B(\omega_\gamma)^2}} - \sqrt{\frac{\phi_{\delta 2}}{p_A p_B(\omega_\gamma)^2}}\right)$$

$$= 1 - 2p_A^t + \frac{\Delta\delta}{\Delta\delta_\gamma} + \Delta\mathrm{p}_{A\to B}^t + p_B\Delta\mathrm{p}_{A\to B}^t + p_A\Delta\mathrm{p}_{A\to B}^p \quad \text{(S30)}$$

Since all populations should be ranged between 0 and 1 ($0 \le p_A^t, p_A^p, p_A^m, p_B^t, p_B^p, p_B^m \le 1$) and all equations are related with p_A^t, one may find more restrictions as follows:

$$0 \le p_A^t \le 1 \quad \text{(S31)}$$

$$0 \le p_A^p = p_A^t - \frac{\Delta\delta}{\Delta\delta_\gamma} - p_B\left(\Delta\mathrm{p}_{A\to B}^t - \Delta\mathrm{p}_{A\to B}^p\right) \le 1 \quad \text{(S32)}$$

$$0 \le p_A^m = 1 - 2p_A^t + \frac{\Delta\delta}{\Delta\delta_\gamma} + p_B\left(\Delta\mathrm{p}_{A\to B}^t - \Delta\mathrm{p}_{A\to B}^p\right) \le 1 \quad \text{(S33)}$$

$$0 \le p_B^t = p_A^t - \Delta\mathrm{p}_{A\to B}^t \le 1 \quad \text{(S34)}$$

$$0 \le p_B^p = p_A^t - \frac{\Delta\delta}{\Delta\delta_\gamma} - p_B\Delta\mathrm{p}_{A\to B}^t - p_A\Delta\mathrm{p}_{A\to B}^p \le 1 \quad \text{(S35)}$$

$$0 \le p_B^m = 1 - 2p_A^t + \frac{\Delta\delta}{\Delta\delta_\gamma} + \Delta\mathrm{p}_{A\to B}^t + p_B\Delta\mathrm{p}_{A\to B}^t + p_A\Delta\mathrm{p}_{A\to B}^p \le 1 \quad \text{(S36)}$$

Solving the inequalities for p_A^t gives six constraints for p_A^t as follows:

$$0 \le p_A^t \le 1 \quad \text{(S37)}$$

$$\frac{\Delta\delta}{\Delta\delta_\gamma} + p_B\left(\Delta\mathrm{p}_{A\to B}^t - \Delta\mathrm{p}_{A\to B}^p\right) \le p_A^t \le 1 + \frac{\Delta\delta}{\Delta\delta_\gamma} + p_B\left(\Delta\mathrm{p}_{A\to B}^t - \Delta\mathrm{p}_{A\to B}^p\right) \quad \text{(S38)}$$

$$\frac{\left(\frac{\Delta\delta}{\Delta\delta_\gamma} + p_B\left(\Delta\mathrm{p}_{A\to B}^t - \Delta\mathrm{p}_{A\to B}^p\right)\right)}{2} \le p_A^t \le \frac{\left(1 + \frac{\Delta\delta}{\Delta\delta_\gamma} + p_B\left(\Delta\mathrm{p}_{A\to B}^t - \Delta\mathrm{p}_{A\to B}^p\right)\right)}{2} \quad \text{(S39)}$$

$$\Delta\mathrm{p}_{A\to B}^t \le p_A^t \le 1 + \Delta\mathrm{p}_{A\to B}^t \quad \text{(S40)}$$

$$\frac{\Delta\delta}{\Delta\delta_\gamma} + p_B\Delta\mathrm{p}_{A\to B}^t + p_A\Delta\mathrm{p}_{A\to B}^p \le p_A^t \le 1 + \frac{\Delta\delta}{\Delta\delta_\gamma} + p_B\Delta\mathrm{p}_{A\to B}^t + p_A\Delta\mathrm{p}_{A\to B}^p \quad \text{(S41)}$$

$$\frac{\left(\frac{\Delta\delta}{\Delta\delta_\gamma} + \Delta\mathrm{p}_{A\to B}^t + p_B\Delta\mathrm{p}_{A\to B}^t + p_A\Delta\mathrm{p}_{A\to B}^p\right)}{2} \le p_A^t \le \frac{\left(1 + \frac{\Delta\delta}{\Delta\delta_\gamma} + \Delta\mathrm{p}_{A\to B}^t + p_B\Delta\mathrm{p}_{A\to B}^t + p_A\Delta\mathrm{p}_{A\to B}^p\right)}{2} \quad \text{(S42)}$$

In order to fulfill these six limits, the maximum value of all six lower limits (left side of equations) should be smaller than the minimum value of all six upper limits (right side of equations). To determine the ranges of allowable population values and conditional population values, a grid search of p_A values was performed from 0.001 to 0.999 in

increments of 0.001. If the six limits above could be fulfilled for a given p_A value, then both the conditional populations (p_A^t, p_A^p, etc.) and populations ($p_A p_A^t$, $p_A p_A^p$, etc.) were evaluated for the lowest and highest allowable p_A^t values at that p_A value. The ranges were calculated from the set of all values determined during the grid search (Figure S7-8).

Populations for valine can also be modeled with similar equations:

$$\delta_1 = p_A p_A^t \delta_t + p_A p_A^p \delta_g + p_A p_A^m \delta_t + p_B p_B^t \delta_t + p_B p_B^p \delta_g + p_B p_B^m \delta_t \quad \text{(S43)}$$

$$\delta_2 = p_A p_A^t \delta_t + p_A p_A^p \delta_t + p_A p_A^m \delta_g + p_B p_B^t \delta_t + p_B p_B^p \delta_t + p_B p_B^m \delta_g \quad \text{(S44)}$$

$$\Delta\delta = \delta_2 - \delta_1 = p_A p_A^p \Delta\delta_\gamma - p_A p_A^m \Delta\delta_\gamma + p_B p_B^p \Delta\delta_\gamma - p_B p_B^m \Delta\delta_\gamma \quad \text{(S45)}$$

$$\Delta\delta = [(p_A p_A^p + p_B p_B^p) - (p_A p_A^m + p_B p_B^m)]\Delta\delta_\gamma \quad \text{(S46)}$$

$$\Delta \mathrm{p}_{A\to B}^p = p_A^p - p_B^p = \pm\sqrt{\frac{\phi_{ex,1}}{p_A p_B (\omega_\gamma)^2}} \quad \text{(S47)}$$

$$\Delta \mathrm{p}_{A\to B}^m = p_A^m - p_B^m = \pm\sqrt{\frac{\phi_{ex,2}}{p_A p_B (\omega_\gamma)^2}} \quad \text{(S48)}$$

A comparison of equations S21-S24 with equations S45-S48 shows that valine can be modeled with the same equations as leucine if the definition of $\Delta\delta$ is reversed before modeling, and by mapping the leucine t, p, and m rotameric states to valine m, p, and t, respectively.

Supplementary Tables

Table S1. Rotameric states for leucine methyl groups from the δ position chemical shifts that showed a contribution of exchange from the methyl ^{13}C RD experiments.

Protein	Residue	p_{trans} [a]	$p_{gauche+}$	δ1 CSV (ppm)[b]	δ2 CSV (ppm)[b]
Ubiquitin	Leu15	0.82	0.18	23.31	20.07
	Leu43	0.72	0.28	22.59	20.41
	Leu50	1.00	0.00	22.14	15.60
	Leu56	0.87	0.13	22.95	19.23
	Leu71	0.59	0.41	21.09	20.23
GB3	Leu5	0.40	0.60	20.83	21.77
	Leu12	0.66	0.34	21.33	19.73

[a] Calculated using the relation $^{13}C(\delta 1) - {}^{13}C(\delta 2) = -5 + 10\,p_t$ [37]

[b] Chemical shift value (CSV) for ubiquitin and GB3 leucine methyl resonances at 277 K and 275 K, respectively

Table S2. Comparison of calculated and experimental conformational amplitudes (Φ_{ex}) for observed residues in ubiquitin and GB3.

Theoretical Φ_{ex} values calculated using the 3-state inter rotamer model.

Protein	Residue	Theoretical Φ_{ex} (ppm^2)	Theoretical Φ_{ex} (ppm^2) ± 30° deviation from ideal geometry[a]	Theoretical Φ_{ex} (ppm^2)	Theoretical Φ_{ex} (ppm^2) ± 30° deviation from ideal geometry[a]	Experimental Φ_{ex} (ppm^2)
Ubiquitin	V5γ1	0.18[b]	0.44-0.15[b]	0.85[c]	1.20-0.95[c]	0.022 ± 0.003
	V70γ2	0.39[b]	0.53-0.07[b]	0.23[c]	1.16-0.10[c]	0.015 ± 0.003
GB3	V6γ1	0.10[b]	0.10-0.16[b]	0.44[d]	0.35-1.06[d]	0.018 ± 0.002
	V21γ1	-	-	3.18[d]	0.34-6.87[d]	0.018 ± 0.004
	V39γ2	0.20[b]	0.24-1.33[b]	0.18[d]	0.58-1.97[d]	0.046 ± 0.020
	V42γ1	1.00[b]	0.86-2.17[b]	1.20[d]	1.22-2.04[d]	0.029 ± 0.001
	V54γ2	3.09[b]	1.70-1.53[b]	0.10[d]	0.38-2.41[d]	0.064 ± 0.005

[a] The range represents the Φ_{ex} calculated with chemical shifts that deviate by ± 30° from ideal geometry.

[b] Populations from Chou et al.[34]

[c] Populations from Fares et al.[12]

[d] Populations from Hansen et al.[32]

Theoretical Φ_{ex} values calculated assuming a two-state exchange model for leucine residues that had observable RD.

Protein	Residue	p_{trans}	$p_{gauche+}$	Theoretical Φ_{ex} (ppm^2)	Experimental Φ_{ex} (ppm^2)
Ubiquitin	L15δ1	0.82	0.18	4.46	0.024 ± 0.004
	L43δ	0.72	0.28	6.10	0.048 ± 0.004 / 0.031 ± 0.003 (δ1/ δ2)
	L50δ2	1.00	0.00	0.00	0.134 ± 0.005
	L56δ2	0.87	0.13	3.42	0.211 ± 0.006
	L71δ2	0.59	0.41	7.32	0.016 ± 0.003
GB3	L5δ1	0.40	0.60	7.26	0.028 ± 0.016
	L12δ	0.66	0.34	6.79	0.053 ± 0.006 / 0.122 ± 0.037 (δ1/ δ2)

Theoretical Φ_{ex} values calculated assuming a two-state exchange model with populations derived from chemical shifts[35] for isoleucine residues that had observable RD[a].

Protein	Residue	p_{trans} (293 K)	$p_{gauche-}$ (293 K)	Theoretical Φ_{ex} (ppm^2)	Experimental Φ_{ex} (ppm^2)
Ubiquitin	I23δ	0.04	0.96	1.06	0.024 ± 0.002
	I44δ	0.62	0.38	7.14	0.052 ± 0.002

[a] At 277 K, chemical shifts indicate that for both I23δ and I44δ $p_{gauche-}$ is populated at 100% based on the model by Hansen et al[35].

Theoretical Φ_{ex} values calculated assuming a two-state exchange model with populations derived from Fares et al[12] for isoleucine residues that had observable RD.

Protein	Residue	p_{trans}	$p_{gauche-}$	Theoretical Φ_{ex} (ppm^2)	Experimental Φ_{ex} (ppm^2)
Ubiquitin	I23δ	--	--	--	--
	I44δ	0.1	0.9	2.723	0.052 ± 0.002

Theoretical Φ_{ex} values calculated assuming a two-state exchange model with populations derived from Chou et al[34] for isoleucine residues that had observable RD.

Protein	Residue	p_{trans}	$p_{gauche-}$	Theoretical Φ_{ex} (ppm^2)	Experimental Φ_{ex} (ppm^2)
Ubiquitin	I23δ	0.07 ± 0.06	0.89 ± 0.04	1.885 ± 1.700	0.024 ± 0.002
	I44δ	0.06 ± 0.02	0.91 ± 0.01	1.652 ± 0.569	0.052 ± 0.002

Table S3. Comparison of overall rotamer populations for observed valines in ubiquitin and GB3

Protein	Res	p_{trans}				$p_{gauche+}$				$p_{gauche-}$			
		PS[a]	CS[b]	SC[c]	RDC[d]	PS[a]	CS[b]	SC[c]	RDC[d]	PS[a]	CS[b]	SC[c]	RDC[d]
Ubiquitin	V5	0.00-0.73	0.76*	0.94*	0.92*	0.00-0.37	0.24	0.06	0.02	0.26-0.63	0.00*	0.00*	0.06*
	V70	0.00-0.81			0.36	0.00-0.41			0.05	0.19-0.59			0.59
GB3	V6	0.00-0.95	0.76	0.90	0.81	0.05-0.52	0.15	0.05	0.01	0.00-0.47	0.10	0.05	0.18
	V21	0.00-0.82	0.39	0.16	0.50	0.00-0.41	0.20	0.35	0.00	0.18-0.59	0.41	0.50	0.50
	V39	0.00-0.98	0.95	0.80	0.77	0.00-0.49	0.00	0.15	0.10	0.02-0.51	0.05	0.06	0.13
	V42	0.00-0.99	0.94	0.71	0.80	0.00-0.50	0.01	0.14	0.12	0.00-0.50	0.06	0.16	0.08
	V54	0.00-0.86	0.47	0.19	0.01	0.14-0.56	0.35	0.82*	0.79*	0.00-0.43	0.19	0.00	0.20

[a] Population ranges derived from modeling of population shuffling (Figure S7-S8)

[b] Populations from Hansen et al.[32] chemical shifts

[c] Populations from Hansen et al.[32] scalar couplings

[d] Populations from Chou et al.[34] RDCs

[*] Population value outside range derived from modeling of population shuffling

Supplementary Figures

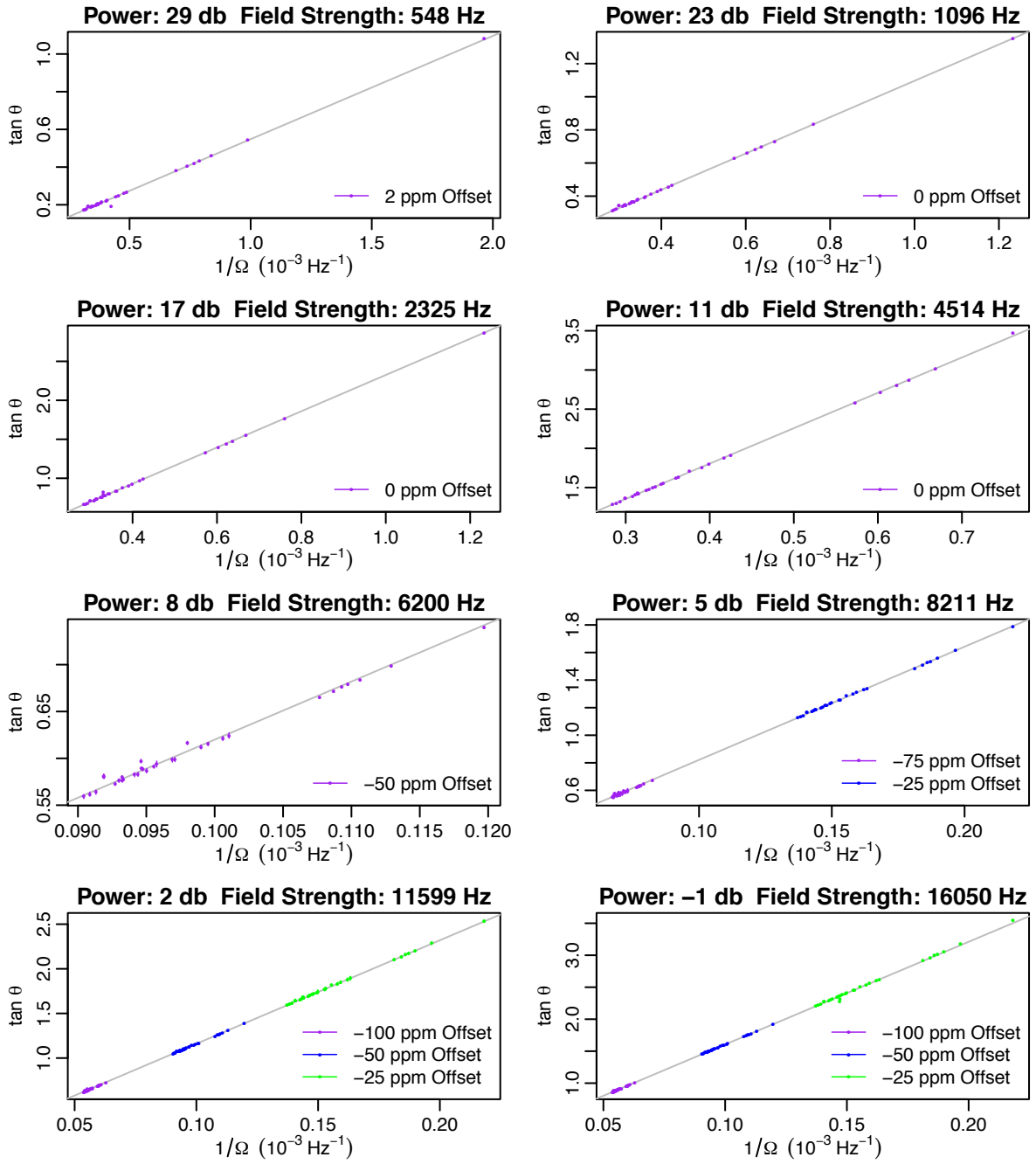

Figure S1. Field strength calibrations for methyl ^{13}C experiments.

This shows that field strengths up to 16 kHz can be applied using a cryogenically cooled probe head. Continuous wave decoupling (CW) was applied at different offsets (represented by different colors) from the center of the ^{13}C spectrum. Different CW decoupling powers were applied, with each plot showing all the data at a given power. Each data point represents an individual resonance. Ω is the frequency difference between a given resonance and the position of the applied CW decoupling and θ is the measured tilt angle. $\tan\theta$ was determined using the equation $\tan\theta = \sqrt{(J_0/J_R)^2 - 1}$, where J_0 is the proton scalar coupling (without CW decoupling) and J_R is the reduced scalar coupling produced by CW decoupling. The line

of best fit (intercept fixed at 0) is shown in gray with slope (Hz) in the title. Errors in peak positions were estimated using peak width divided by signal to noise. Most of the propagated errors (vertical lines) do not exceed the height of the plotting point. All experiments were conducted at 277 K using a Bruker QCI cryroprobe with a spectrometer operating at a Larmor frequency of 600 MHz.

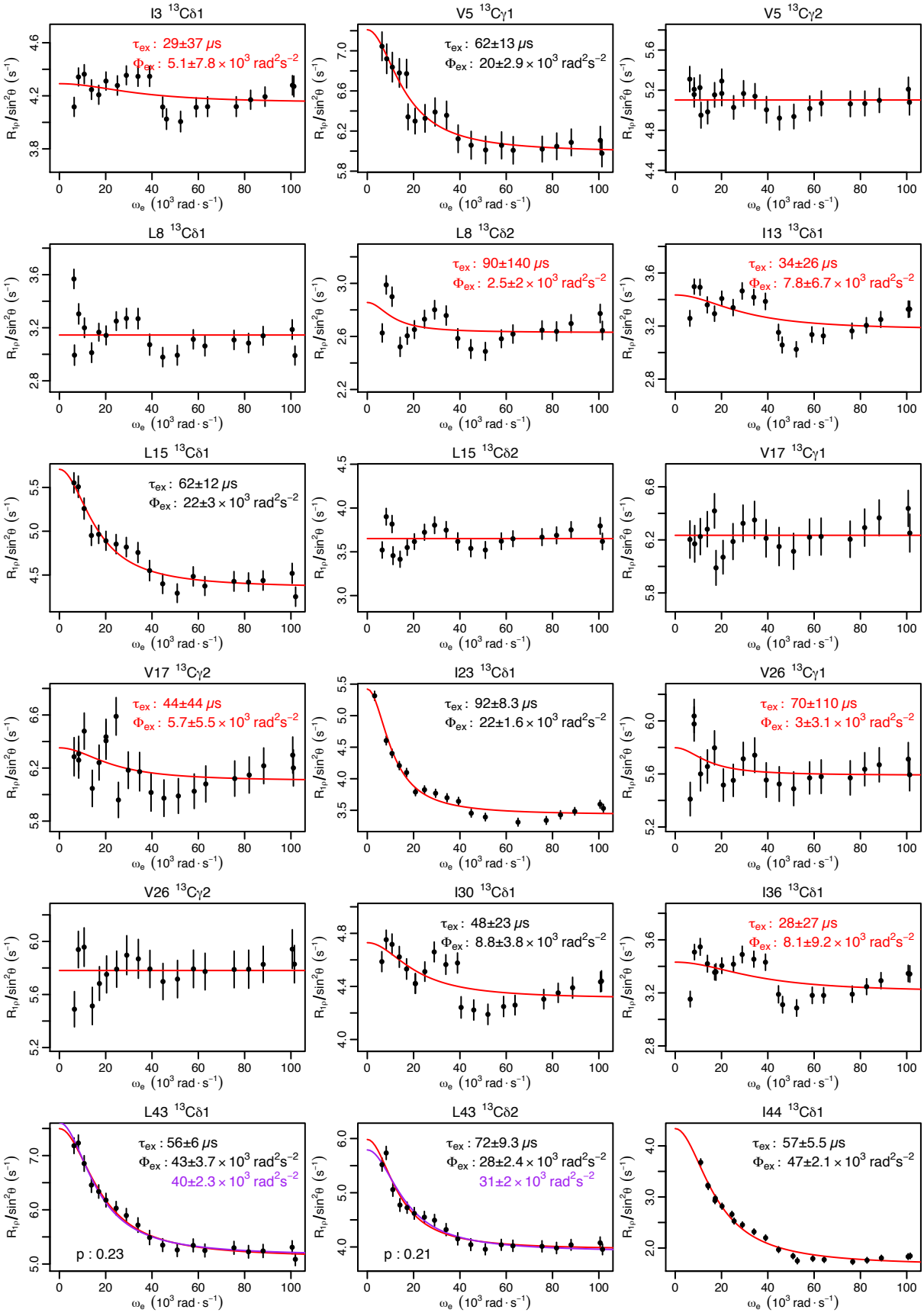
I3 13Cδ1
τex : 29±37 μs
Φex : 5.1±7.8 × 10^3 rad^2s^-2
V5 13Cγ1
τex : 62±13 μs
Φex : 20±2.9 × 10^3 rad^2s^-2
V5 13Cγ2
L8 13Cδ1
L8 13Cδ2
τex : 90±140 μs
Φex : 2.5±2 × 10^3 rad^2s^-2
I13 13Cδ1
τex : 34±26 μs
Φex : 7.8±6.7 × 10^3 rad^2s^-2
L15 13Cδ1
τex : 62±12 μs
Φex : 22±3 × 10^3 rad^2s^-2
L15 13Cδ2
V17 13Cγ1
V17 13Cγ2
τex : 44±44 μs
Φex : 5.7±5.5 × 10^3 rad^2s^-2
I23 13Cδ1
τex : 92±8.3 μs
Φex : 22±1.6 × 10^3 rad^2s^-2
V26 13Cγ1
τex : 70±110 μs
Φex : 3±3.1 × 10^3 rad^2s^-2
V26 13Cγ2
I30 13Cδ1
τex : 48±23 μs
Φex : 8.8±3.8 × 10^3 rad^2s^-2
I36 13Cδ1
τex : 28±27 μs
Φex : 8.1±9.2 × 10^3 rad^2s^-2
L43 13Cδ1
τex : 56±6 μs
Φex : 43±3.7 × 10^3 rad^2s^-2
40±2.3 × 10^3 rad^2s^-2
p : 0.23
L43 13Cδ2
τex : 72±9.3 μs
Φex : 28±2.4 × 10^3 rad^2s^-2
31±2 × 10^3 rad^2s^-2
p : 0.21
I44 13Cδ1
τex : 57±5.5 μs
Φex : 47±2.1 × 10^3 rad^2s^-2
R1ρ/sin^2θ (s^-1)
ωe (10^3 rad·s^-1)

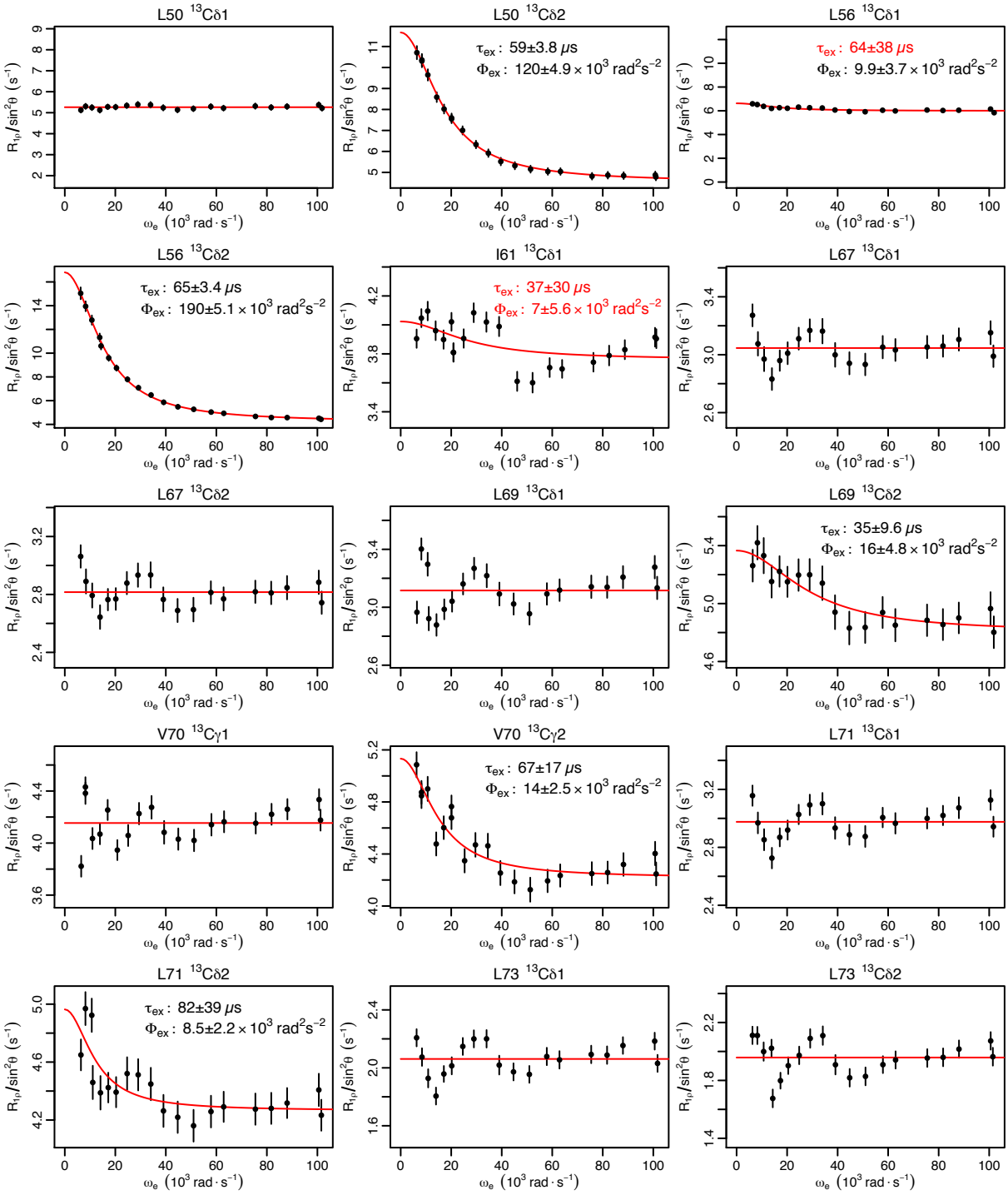

Figure S2. Methyl ^{13}C $R_{1\rho}$ data for ubiquitin nuclei.

The fit to equation S1 is shown in red, with corresponding τ_{ex} and Φ_{ex} parameter values shown in black. For the two L43 methyl ^{13}C nuclei, that equation was also fit with a single τ_{ex} (61 μs), shown in purple. The corresponding Φ_{ex} parameter values from the joint fit are shown in purple. The p-value shown is from an F-test between the two fits, indicating that the individual fits are not significantly better than the joint fit. If the error of a fit parameter exceeded half the value, it is colored red and the RD was considered insignificant (see Materials and Methods). If the fitting procedure did not converge, a red horizontal line with the mean $R_{1\rho}/\sin^2\theta$ value is shown without parameters. Minor oscillations (on the order of ±0.2 s^{-1}) are present in the data for some residues.

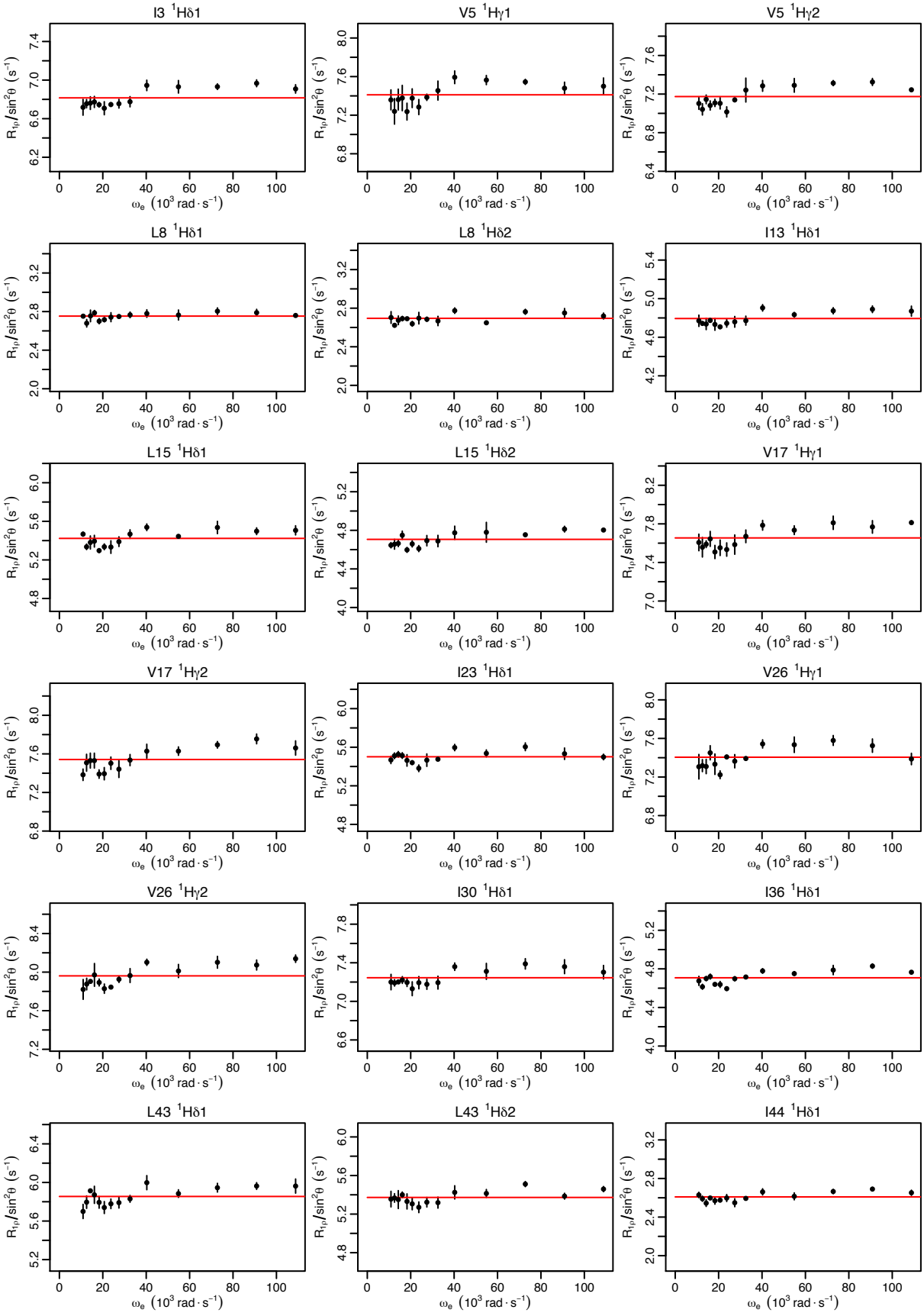
I3 ^{1}Hδ1
V5 ^{1}Hγ1
V5 ^{1}Hγ2
L8 ^{1}Hδ1
L8 ^{1}Hδ2
I13 ^{1}Hδ1
L15 ^{1}Hδ1
L15 ^{1}Hδ2
V17 ^{1}Hγ1
V17 ^{1}Hγ2
I23 ^{1}Hδ1
V26 ^{1}Hγ1
V26 ^{1}Hγ2
I30 ^{1}Hδ1
I36 ^{1}Hδ1
L43 ^{1}Hδ1
L43 ^{1}Hδ2
I44 ^{1}Hδ1
$R_{1\rho}/\sin^2\theta$ (s^{-1})
ω_e (10^3 rad·s^{-1})

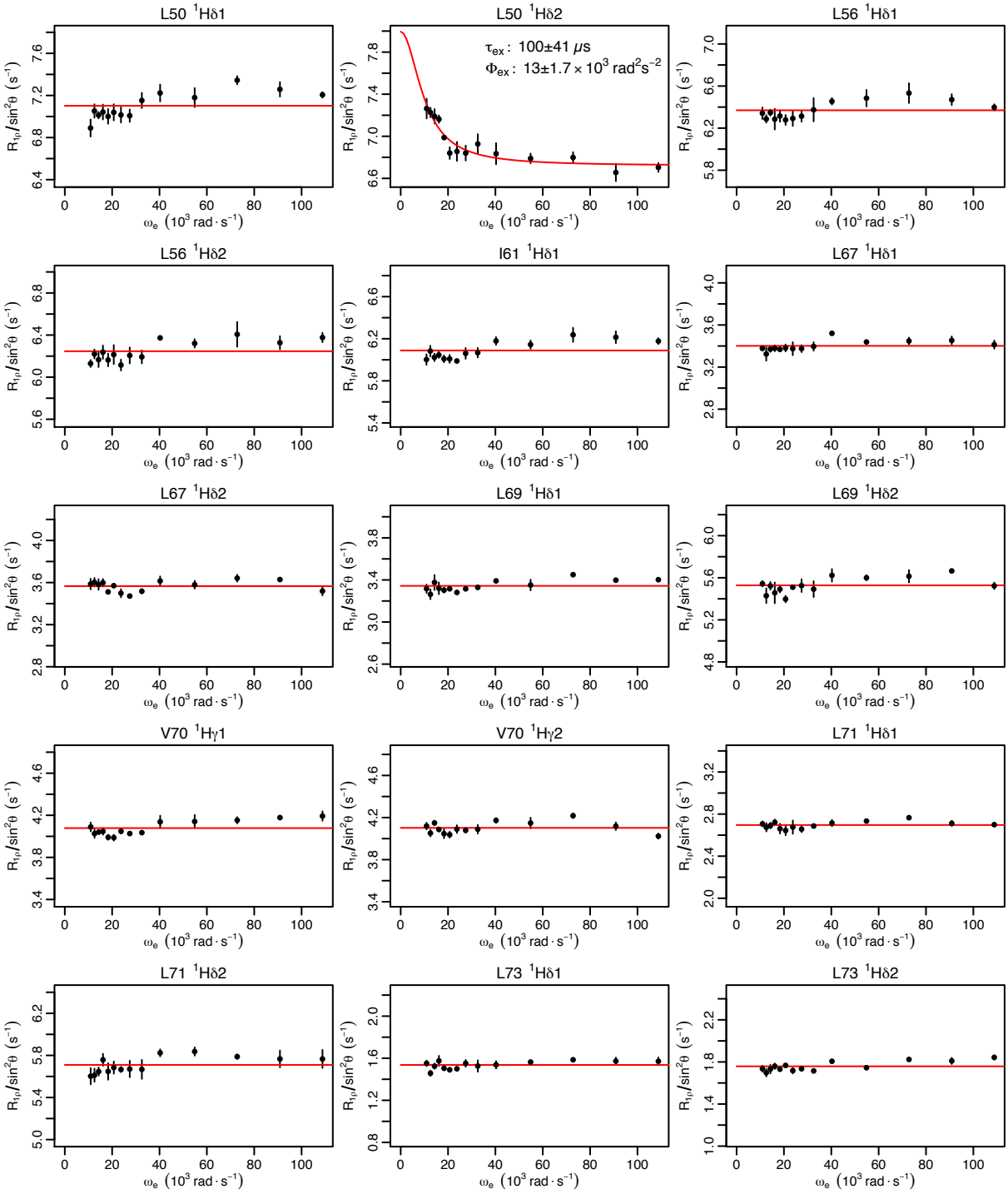

Figure S3. Methyl ^{1}H $R_{1\rho}$ data for ubiquitin nuclei.

The fit to equation S1 is shown in red, with corresponding τ_{ex} and Φ_{ex} parameter values shown in black. If the error of a fit parameter exceeded half the value, it is colored red and the RD was considered insignificant (see Materials and Methods). If the fitting procedure did not converge, a red horizontal line with the mean $R_{1\rho}/\sin^2\theta$ value is shown without parameters.

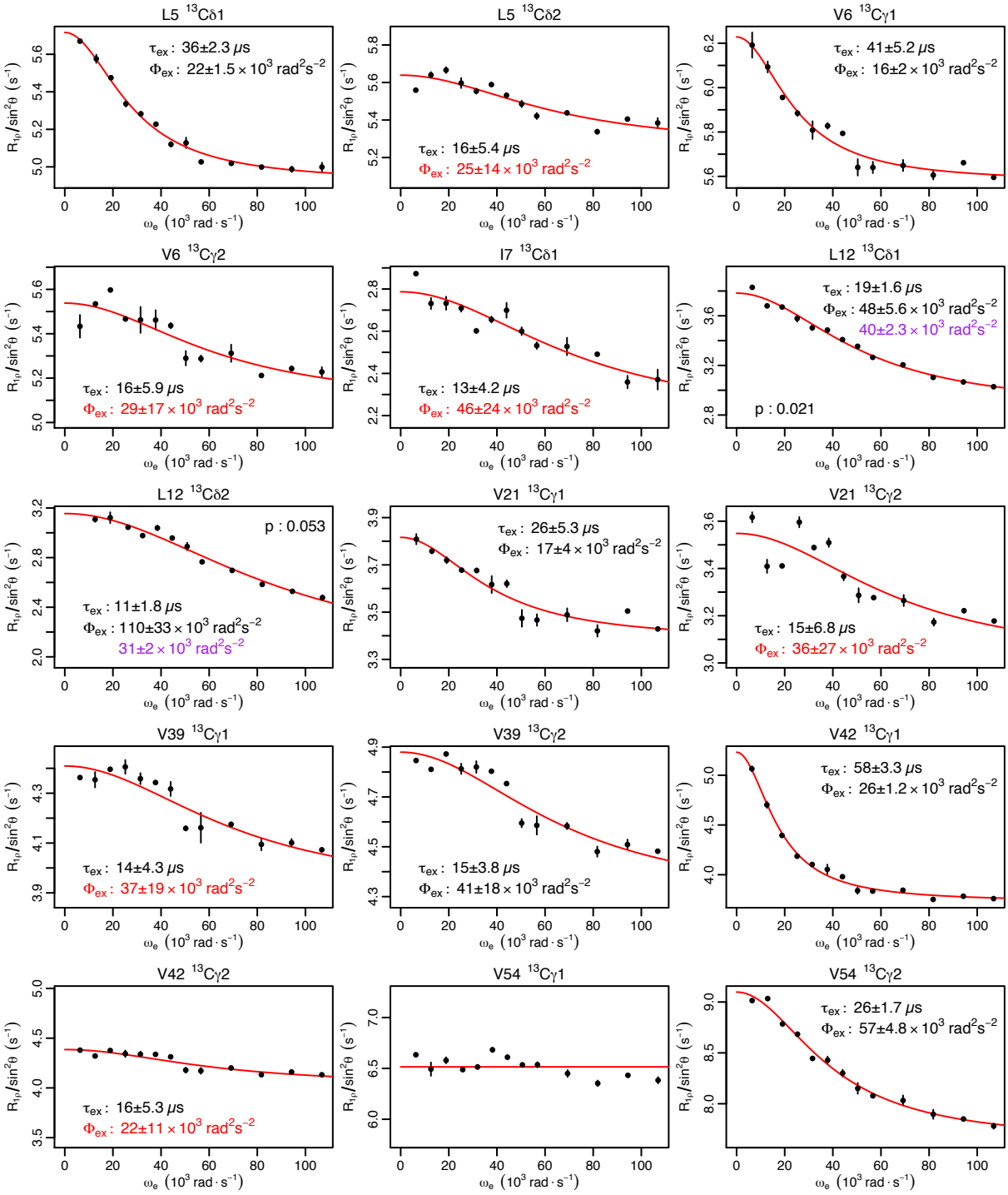

Figure S4. Methyl ^{13}C $R_{1\rho}$ data for GB3 nuclei.

The fit to equation S1 is shown in red, with corresponding τ_{ex} and Φ_{ex} parameter values shown in black. For the two L12 methyl ^{13}C nuclei, that equation was also fit with a single τ_{ex} (15 μs), shown in purple. The corresponding Φ_{ex} parameter values from the joint fit are shown in purple. The p-value shown is from an F-test between the two fits, indicating that the individual fits are not significantly better than the joint fit. If the error of a fit parameter exceeded half the value, it is colored red and the RD was considered insignificant (see Materials and Methods). If the fitting procedure did not converge, a red horizontal line with the mean $R_{1\rho}/\sin^2\theta$ value is shown without parameters.

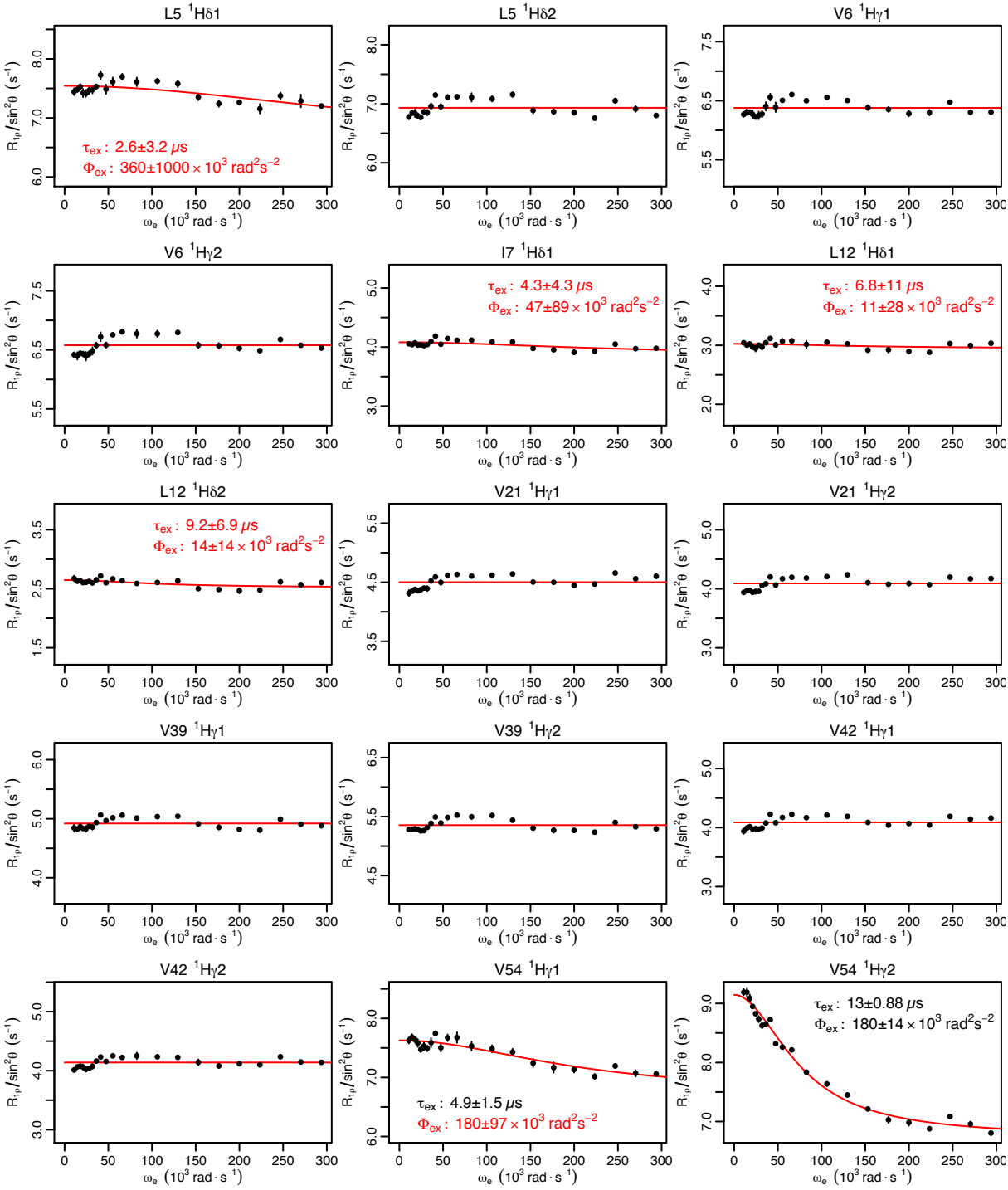

Figure S5. Methyl ^{1}H $R_{1\rho}$ data for GB3 nuclei.

The fit to equation S1 is shown in red, with corresponding τ_{ex} and Φ_{ex} parameter values shown in black. If the error of a fit parameter exceeded half the value, it is colored red and the RD was considered insignificant (see Materials and Methods). If the fitting procedure did not converge, a red horizontal line with the mean $R_{1\rho}/\sin^2\theta$ value is shown without parameters.

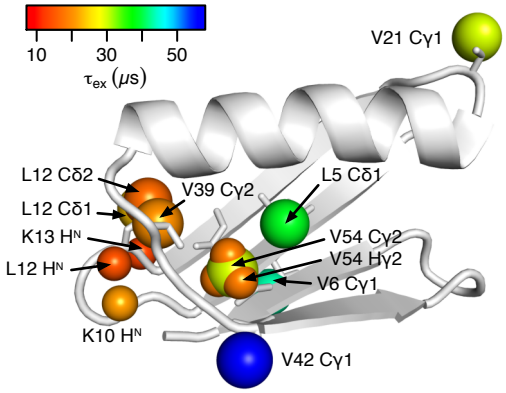

Figure S6. GB3 timescales are spatially correlated.

Backbone and side chain nuclei with significant RD are shown as spheres, with isoleucine, leucine, and valine residues shown as sticks. The nuclei are colored by τ_{ex}. There is a general spatial correlation to the τ_{ex} values. This suggests that there might be a faster timescale process primarily affecting nuclei on the left, and a slower timescale process primarily affecting nuclei on the right. Some nuclei may be affected by both processes, which would produce intermediate τ_{ex} values during the fitting process.

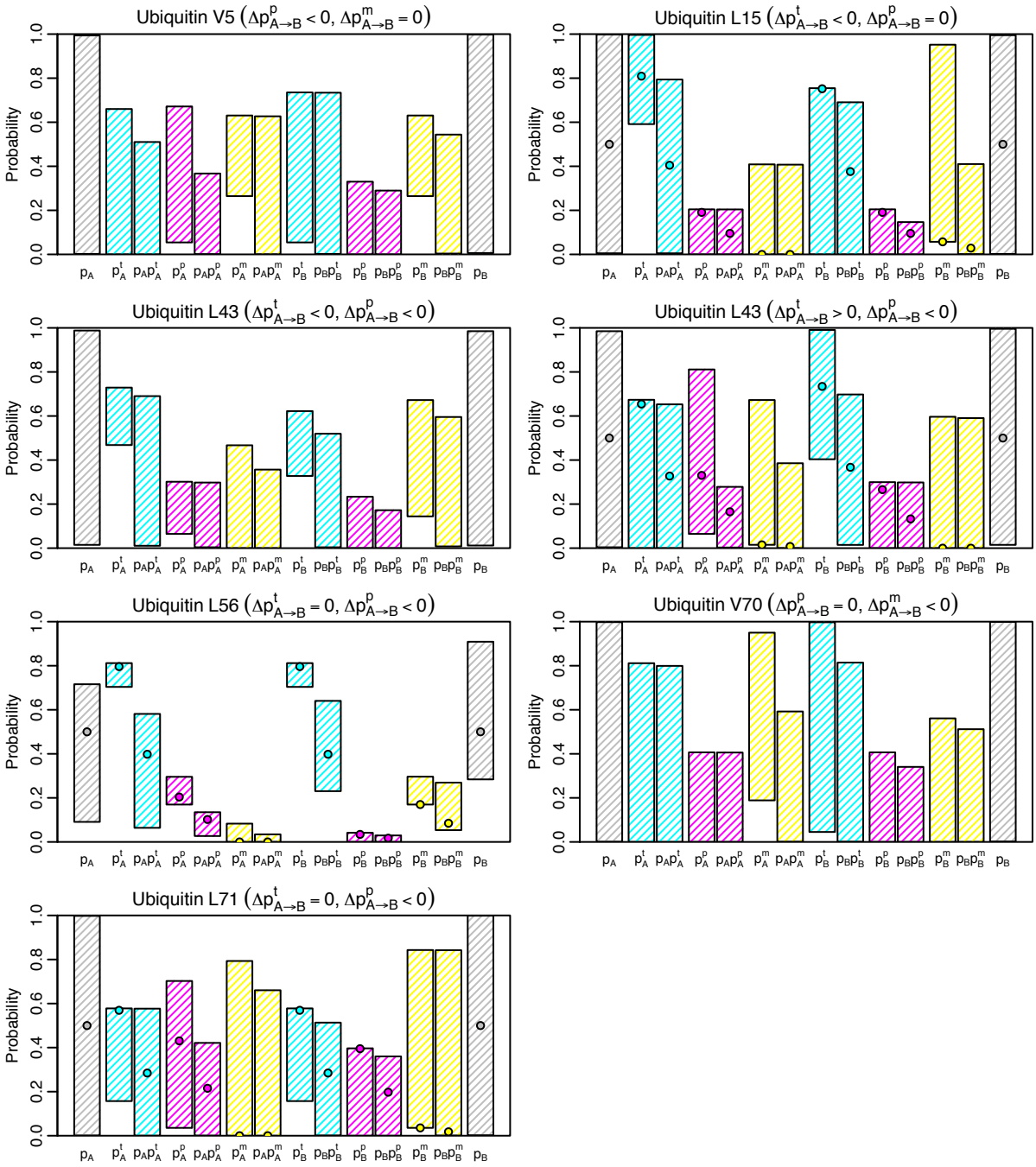

Figure S7. Models of ubiquitin side chain populations for leucine and valine residues.

Possible values of populations (p_i and $p_i p_i^j$) and conditional probabilities (p_i^j) are given by the hashed areas. The models were fit assuming no error, so the uncertainty results entirely from the underdetermined system of equations. L50 is not modeled because the large methyl ^{13}C chemical shift difference, most likely perturbed by ring current effects from neighboring Y59, suggests that only the trans rotameric state is populated (Table S1). Circles in leucine residues indicate the populations for which $p_A = p_B$ and $p_i p_i^m$ is minimized. The largest $p_A p_A^m + p_B p_B^m$ is 0.085 and the average over modeled leucines is 0.031. These values are close to a set of free ubiquitin simulations[19], in which the largest and average gauche$^-$ populations were 0.051 and 0.017, respectively.

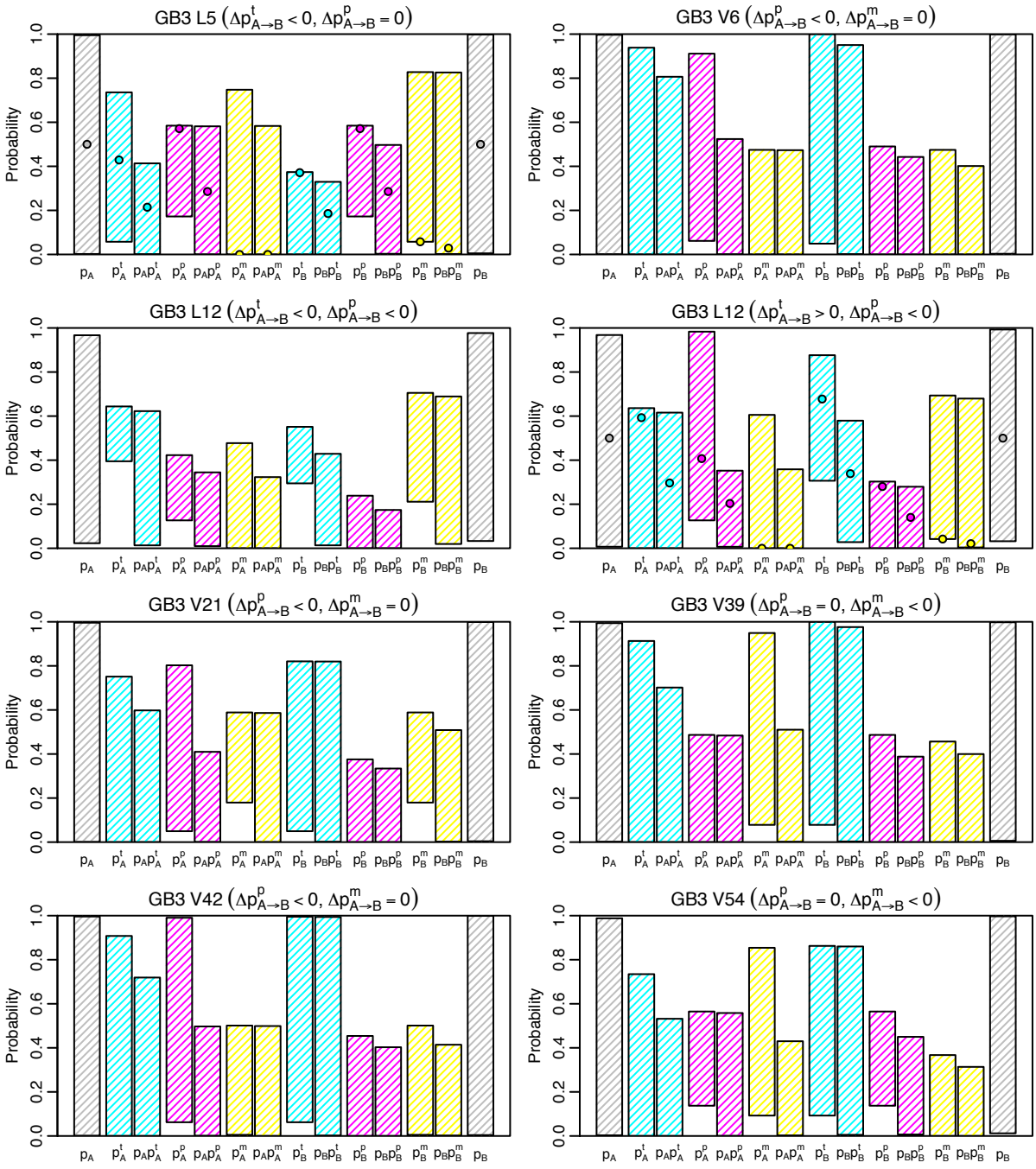

Figure S8. Models of GB3 side chain populations for leucine and valine residues.

Possible values of populations (p_i and $p_i p_i^j$) and conditional probabilities (p_i^j) are given by the hashed areas. The models were fit assuming no error, so the uncertainty results entirely from the underdetermined system of equations. Circles in leucine residues indicate the populations for which $p_A = p_B$ and $p_i p_i^m$ is minimized. The largest $p_A p_A^m + p_B p_B^m$ is 0.023.

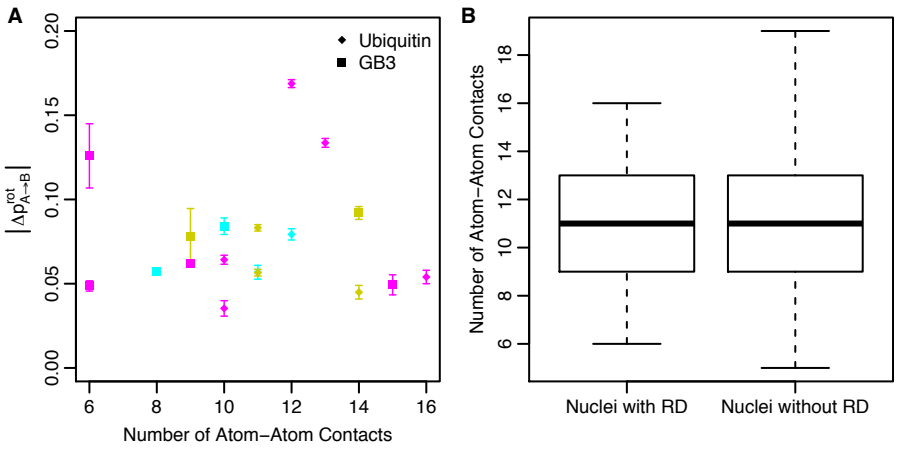

Figure S9. The number of atom-atom contacts is not correlated with population shuffling.

A) The packing density of a given ^{13}C nucleus, in terms of the number of atom-atom contacts[38] is plotted against the population changes derived from that nucleus. Trans, gauche$^+$, and gauche$^-$ rotamer population changes are colored cyan, magenta, and yellow, respectively. **B)** Packing density does not influence whether a nucleus shows RD or not, as shown by a boxplot of atom-atom contacts. The black bar shows the median, the box extends over the interquartile range, and the whiskers extend over the full range.

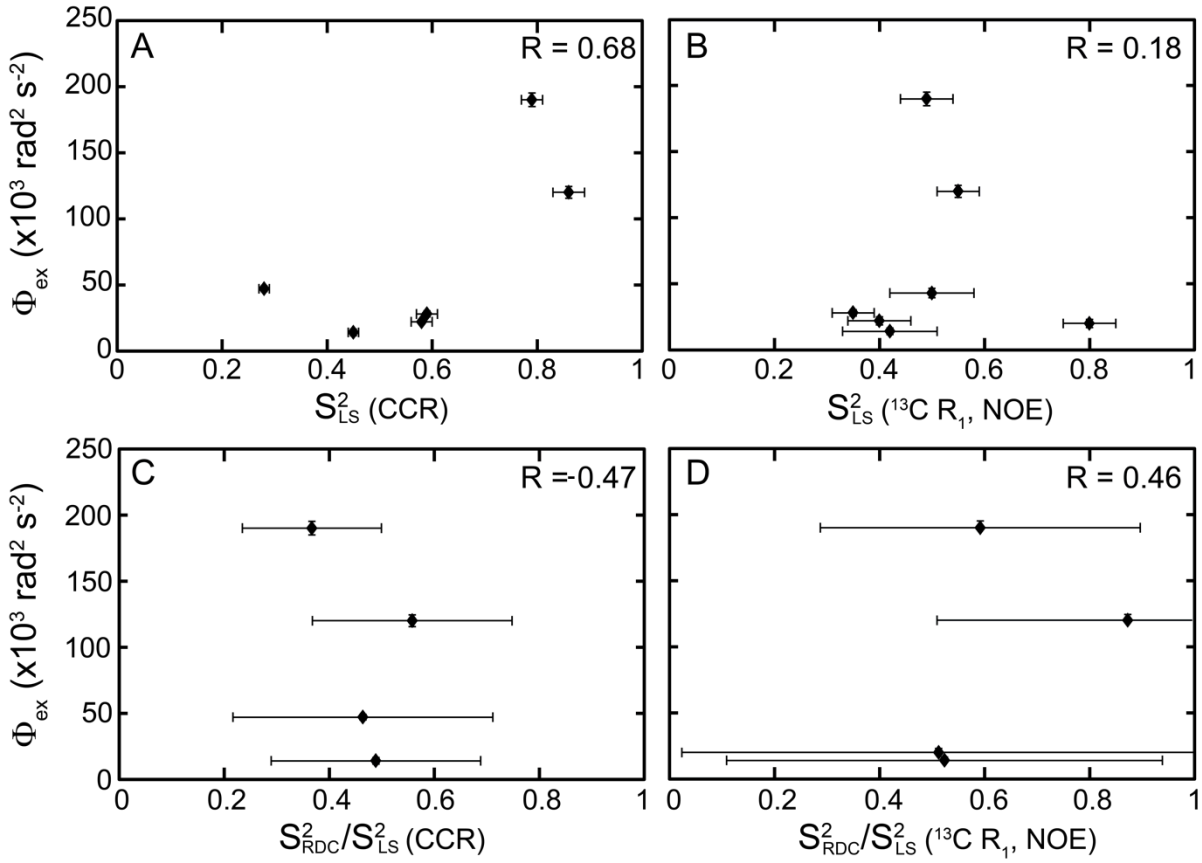

Figure S10. Conformational amplitudes do not correlate with order parameters.

Ubiquitin conformational amplitudes (Φ_{ex}) from methyl ^{13}C $R_{1\rho}$ experiments compared to fast motion order parameters S^2_{LS} derived from **(A)** CCR[39] and ^{13}C **(B)** auto-relaxation experiments[40]. The microsecond process identified by the methyl ^{13}C relaxation dispersion reports on a timescale much slower than the overall tumbling for ubiquitin (τ_c ~10 ns at 277 K) and does not show significant correlation with previously published[39,40] fast-timescale (sub-τ_c) Lipari-Szabo type order parameters that report on a timescale at which rotamer hopping may occur[41]. **(C, D)** Φ_{ex} measured from $R_{1\rho}$ experiments are plotted against the ratio between RDC methyl (S^2_{RDC}) and their Lipari-Szabo (S^2_{LS}) (C[39] and D[40]) order parameters for residues with all available data. Although no correlation exists, all residues show decreased S^2_{RDC} ($S^2_{RDC}/S^2_{LS} < 1$) indicating for observed methyl nuclei with reported order parameters, motion within the supra-τ_c range exists. Whereas methyl ^{13}C $R_{1\rho}$ measured Φ_{ex} report on nuclei being in differentially populated distinct chemical environments, the methyl RDC derived order parameters reflect angular fluctuations of the internuclear vector. In addition, the timescales monitored by RDCs (up to the coalescence limit) and $R_{1\rho}$ Φ_{ex} (exchange effects from 3.4-150 μs) are different. Therefore, it is not surprising that a poor correlation might exist. Errors in the ratio were propagated from the errors of the given sub-τ_c and supra-τ_c order parameters. The Pearson correlation coefficients (R) are given in the plots.

Supplementary References

[28] A. M. Gronenborn, D. R. Filpula, N. Z. Essig, A. Achari, M. Whitlow, P. T. Wingfield, G. M. Clore, *Science* **1991**, 253, 657-661.

[29] G. A. Lazar, J. R. Desjarlais, T. M. Handel, *Protein Sci.* **1997**, 6, 1167-1178.

[30] F. Massi, E. Johnson, C. Wang, M. Rance, A. G. Palmer, *J. Am. Chem. Soc.* **2004**, 126, 2247-2256.

[31] F. A. A. Mulder, de Graaf RA, R. Kaptein, R. Boelens, *J. Magn. Reson.* **1998**, 131, 351-357.

[32] D. F. Hansen, L. E. Kay, *J. Am. Chem. Soc.* **2011**, 133, 8272-8281.

[33] P. Luginbühl, K. Wüthrich, *Prog. Nucl. Magn. Reson. Spectrosc.* **2002**, 40, 199-247.

[34] J. J. Chou, D. A. Case, A. Bax, *J. Am. Chem. Soc.* **2003**, 125, 8959-8966.

[35] D. F. Hansen, P. Neudecker, L. E. Kay, *J. Am. Chem. Soc.* **2010**, 132, 7589-7591.

[36] D. Ban, M. Funk, R. Gulich, D. Egger, T. M. Sabo, K. F. Walter, R. B. Fenwick, K. Giller, F. Pichierri, B. L. de Groot, O. F. Lange, H. Grubmüller, X. Salvatella, M. Wolf, A. Loidl, R. Kree, S. Becker, N. A. Lakomek, D. Lee, P. Lunkenheimer, C. Griesinger, *Angew. Chem. Int. Ed. Engl.* **2011**, 50, 11437-11440.

[37] F. A. Mulder, *Chembiochem* **2009**, 10, 1477-1479.

[38] V. Sobolev, E. Eyal, S. Gerzon, V. Potapov, M. Babor, J. Prilusky, M. Edelman, *Nucleic Acids Res.* **2005**, 33, 39-43.

[39] T. M. Sabo, D. Bakhtiari, K. F. Walter, R. L. McFeeters, K. Giller, S. Becker, C. Griesinger, D. Lee, *Protein Sci.* **2012**, 21, 562-570.

[40] A. L. Lee, P. F. Flynn, A. J. Wand, *J. Am. Chem. Soc.* **1999**, 121, 2891-2902.

[41] N. R. Skrynnikov, O. Millet, L. E. Kay, *J. Am. Chem. Soc.* **2002**, 124, 6449-6460.